5

Rotary Pressure Exchanger for SWRO

Zhou Yihui, Bi Mingshu and Liu Yu
School of Chemical Machinery, Dalian University of Technology, China

1. Introduction

A rotary pressure exchanger (RPE) is a kind of fluid energy recovery equipment which is based on the positive displacement principle. The key components of RPE include a rotor with several circular ducts, two end covers and one sleeve. At any time during operation, half the ducts are exposed to the high pressure fluid and the other half are exposed to the low pressure fluid. There are two indispensable requirements for RPE when used in SWRO: (1) The concentration of fresh seawater at high pressure outward pipe should not be so increased that it will have bad effect on the reverse osmosis. (2) The high pressure system and low pressure system in RPE should be completely separated, otherwise the leakage will happen and lead to the energy recovery efficiency decreases dramatically.

The former one depends on the stable liquid piston which is formed and moves reciprocally in the ducts of rotor. Zhou[1,2] illustrates the dynamics mixing process in the ducts. And the transition process and conditions from initial mixing zone to liquid piston were explained through 2D numerical simulation. The fluid's radial velocity in the duct was neglected during rotation.

The latter requirement depends on the end face seal between rotor and end cover. The face seal of RPE is very difficult for the following reasons: (1) the fluid is seawater which is incompressible and nearly inviscid and (2) the clearance between rotor and end cover has to be existed because it is an indispensable requirement for rotor starting up and rotating. Until now there are no detailed research reports on face seal mechanism of RPE being published.

In this chapter, the primary objective is presented as following :

- The study on the mixing process and the effects of RPE parameters on the liquid piston on the basis 3D model, which will describe the dynamics mixing more accurately and closer to the real operation conditions.
- The study on the face seal with the aim of getting the real seal formation in the clearance of RPE through theoretical analysis and numerical simulation. The results will guide the seal design of RPE experimental equipment. And the effects of clearance on the pressure, leakage and energy recovery are also studied.
- The effects of clearance on energy recovery and mixing rate under different flow and pressure conditions will be studied through RPE energy recovery experiments.

2. 3D Numerical simulation on dynamics mixing in ducts

The 3D model of RPE has a better view on the mixing process between different concentration fluids. The model description is firstly put forward. Then the computational

results are to be illustrated and discussed. Finally, the effects of velocity and rotor speed on the mixing will be discussed.

2.1 Geometry model

In order to verify the validity of model the geometry dimension is in accordance to the real PX equipment[3]. Fig.1 shows the solid model of rotor and endcovers. The length of rotor is 200mm and diameter is 120mm with 12 ducts.

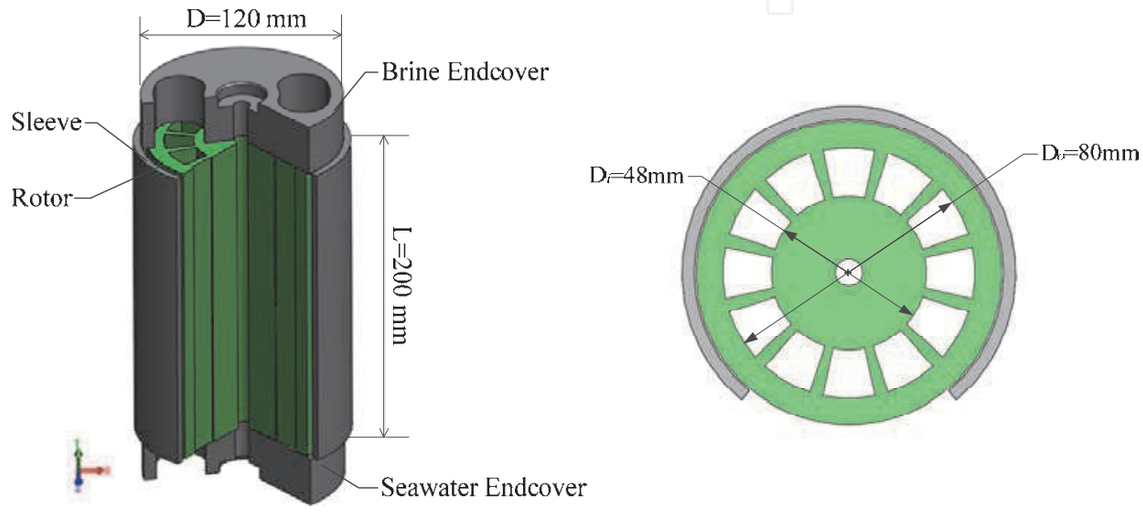

Fig. 1. Geometry model of 3D mixing simulation

2.2 Governing equations and boundary conditions

The numerical simulation is carried out under cylindrical coordination. And the governing equations are[4],

Continuity equation

$$\frac{\partial \rho}{\partial t} + \nabla \cdot (\rho \vec{v}) = 0 \tag{1}$$

Momentum equation[5]

$$\frac{\partial}{\partial t}(\rho \vec{v}) + \nabla \cdot (\rho \vec{v} \vec{v}) = -\nabla P + \nabla \cdot (\bar{\bar{\tau}}) + \rho \vec{g} \tag{2}$$

Where P is the static pressure, $\bar{\bar{\tau}}$ is the stress tensor (described below), and $\rho \vec{g}$ are the gravitational body force.

The stress tensor $\bar{\bar{\tau}}$ is given by

$$\bar{\bar{\tau}} = \mu \left[(\nabla \vec{v} + \nabla \vec{v}^T) - \frac{2}{3} \nabla \cdot \vec{v} I \right] \tag{3}$$

Where μ is the molecular viscosity, *I* is the unit tensor

Specifies equation

$$\frac{\partial}{\partial t}(pY_i) + \nabla \cdot (\rho \vec{v} Y_i) = -\nabla \cdot \vec{J_i} + R_i \tag{4}$$

Where R_i is the net rate of production by chemical reaction and according to the assumption that there is no chemical reaction during the mass transfer.

$$R_i=0$$

In turbulent flows,

$$\vec{J_i} = -\left(\rho D_{i,m} + \frac{\mu_t}{Sc_t}\right)\nabla Y_i - D_{T,i}\frac{\nabla T}{T} \tag{5}$$

Where Sc_t is the turbulent Schmidt number,

$$Sc_t=\frac{\mu_t}{\rho D_t}$$

Where μ_t is the turbulent viscosity and D_t is the turbulent diffusivity. The default Sc_t is 0.7.
Turbulence model:
Turbulent kinetic energy:

$$\frac{\partial}{\partial t}(pk) + \frac{\partial}{\partial x_i}(pku_i) = \frac{\partial}{\partial x_j}\left[(\mu + \frac{\mu_t}{\sigma_k})\frac{\partial k}{\partial x_j}\right] + G_k + G_b - \rho\epsilon - Y_M \tag{6}$$

Where G_b is the generation of turbulence kinetic energy due to buoyancy and Y_m represents the contribution of the fluctuating dilatation in compressible turbulence to the overall dissipation rate,
Turbulent kinetic energy simplified to:

$$\frac{\partial}{\partial t}(pk) + \frac{\partial}{\partial x_i}(pku_i) = \frac{\partial}{\partial x_j}\left[(\mu + \frac{\mu_t}{\sigma_k})\frac{\partial k}{\partial x_j}\right] + G_k + \rho\epsilon \tag{7}$$

Turbulent energy dissipation:

$$\frac{\partial}{\partial t}(\rho\epsilon) + \frac{\partial}{\partial x_i}(\rho\epsilon u_i) = \frac{\partial}{\partial x_j}\left[(\mu + \frac{\mu_t}{\sigma_\epsilon})\frac{\partial \epsilon}{\partial x_j}\right] + C_{1\epsilon}\frac{\epsilon}{k}(G_k + C_{3\epsilon}G_b) - C_{2\epsilon}\rho\frac{\epsilon^2}{k} \tag{8}$$

Where

$$\mu_t = \rho C_\mu \frac{k^2}{\varepsilon}$$

The empirical constants for the RNG k–e model are assigned as following [6]:

$$C_{1\varepsilon} = 1.44, C_{2\varepsilon} = 1.92, C_\mu = 0.09, \sigma_K=1.0, \sigma_\varepsilon = 1.3$$

Boundary conditions
Non-slip boundary condition is used on the inner wall of the duct. The standard wall function method is applied to simulate the flow in the near-wall region. The mass-flow-inlet and pressure-outlet boundary condition are used on the high-pressure brine inlet, low-pressure feed water inlet and high-pressure feed water outlet, low-pressure brine outlet.

And the rotor speed is given by cell zone conditions. Fig.2 shows the computation (a) and grid model (b) ready for the simulation.

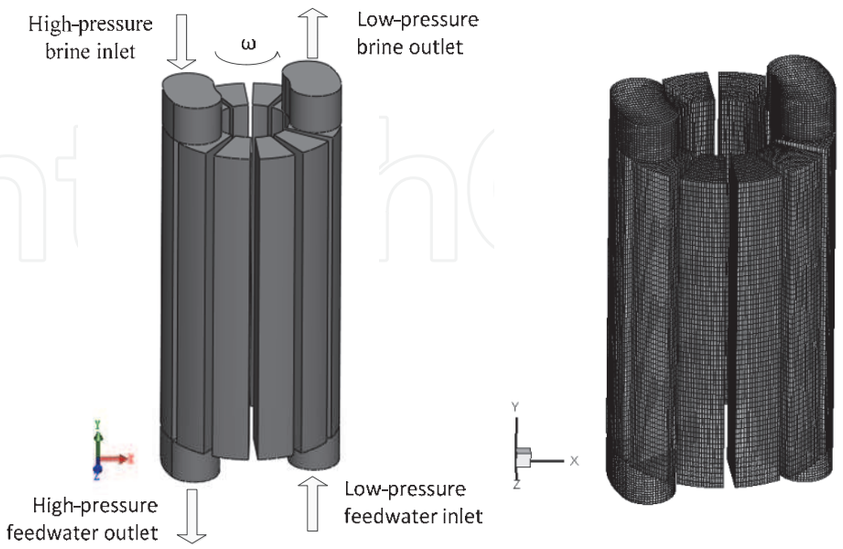

(a)Computation model (b) Grid model

Fig. 2. Geometry model in simulation

2.3 Results and discussion

2.3.1 Verification of 3D model

Fig.3 illustrates the average concentration on the high pressure out surface compared with the ones under real operation conditions[5]. The divergence between those is less than 5%which verifies the numerical model is accurate for the study.

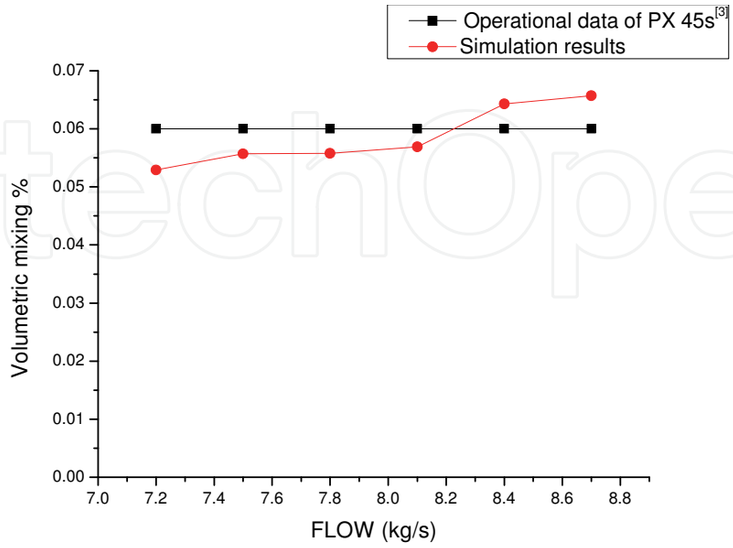

Fig. 3. Comparison between numerical result and real data on high pressure out surface concentration

2.3.2 Liquid piston in the ducts

Fig.4 shows the concentration distribution in all the ducts of rotor. It could be clearly seen that the liquid piston formation in the ducts during rotation. Fig.5 shows the movement of liquid piston separates the fresh water and brine to prevent from over-mixing with each other.

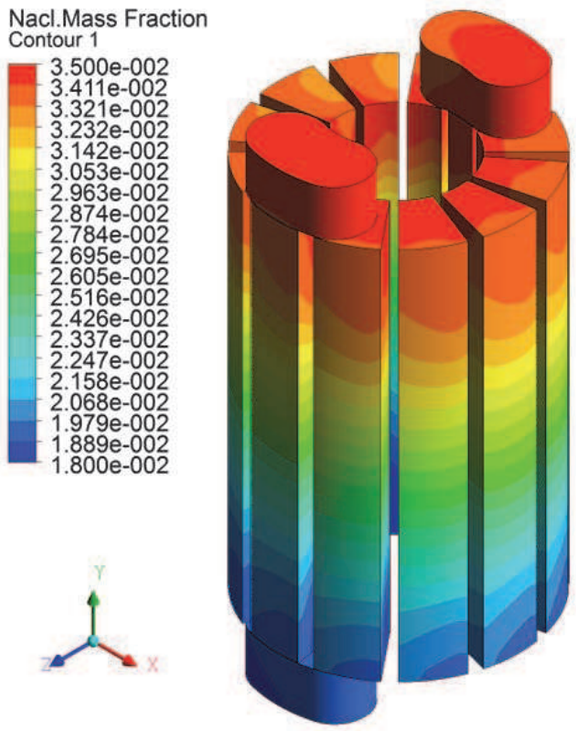

Fig. 4. Concentration distribution in the ducts of rotor

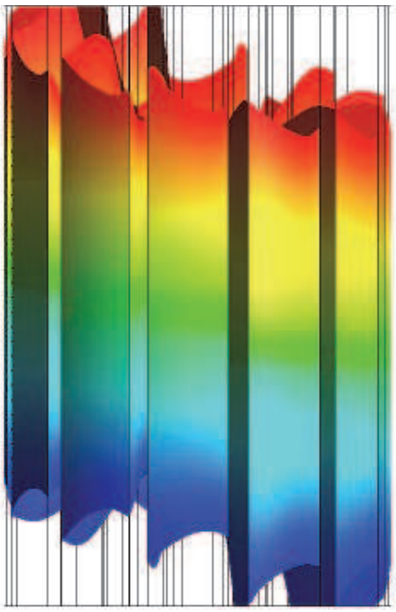

Fig. 5. Liquid piston in the ducts of rotor

2.3.3 Parameters affecting mixing rate

Many parameters affect the mixing rate, in which flow-in velocity and rotation speed are the most important ones. When the rotor was driven by the flow the rotor speed increased with increasing of flow rate linearly. Consequently, the distance of liquid piston moving in the duct almost keep constant because of the effects of velocity and rotor speed on the mixing cancelled with each other[8,9]. While in this chapter, the velocity and rotor speed are studied as independent parameters.

The mixing rate of fresh seawater and concentration stream is calculated according to Eq.(9) and salinity of samples are obtained through electrical conductivity[1].

$$\text{Volumetric Mixing Rate}=\frac{\mathrm{HP}_{\mathrm{out}}-\mathrm{LP}_{\mathrm{in}}}{\mathrm{LP}_{\mathrm{out}}-\mathrm{LP}_{\mathrm{in}}} \tag{9}$$

Fig.6 illustrates the relationship between flow-in velocity and volumetric mixing rate when the rotor speed $\omega = 1200\mathrm{rpm}$. It could be seen from Fig.6 that the mixing rate increases with the increasing of flow-in velocity. And if the mixing rate should be controlled less than 6% the maximum flow-in velocity should not more than $2\mathrm{m/s}$ according to the geometry model and rotor speed.

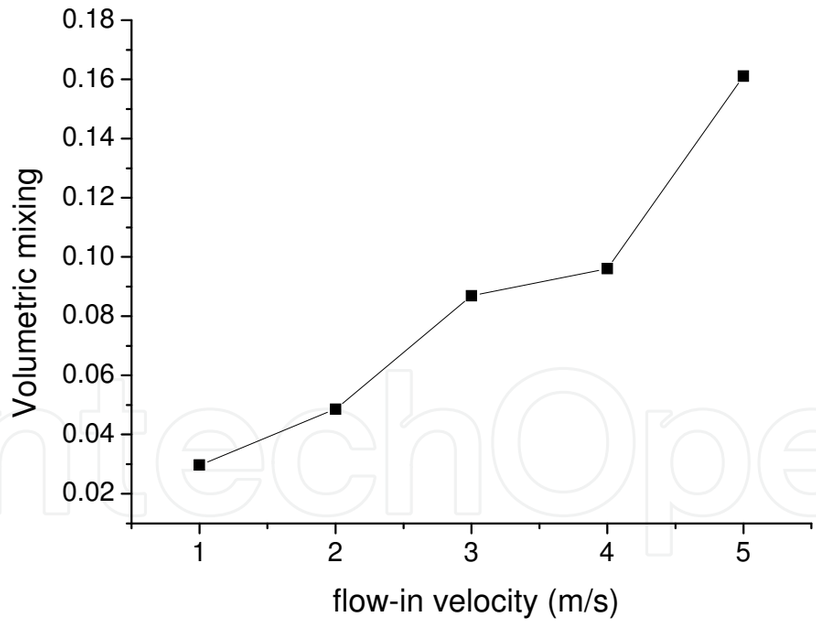

Fig. 6. Relationship between flow-in velocity and mixing rate

Fig.7 is the relationship between rotor speed and mixing rate when the flow-in velocity $v = 2.5\mathrm{m/s}$. It could be seen that with the increasing of rotor speed the mixing rate decreases firstly, and then almost be stable when rotating from 600rpm to 1400rpm. The results show that the mixing rate will be out of control if the rotor speed is low. However, the rotor speed has little effect on the mixing rate once it is more than 800rpm.

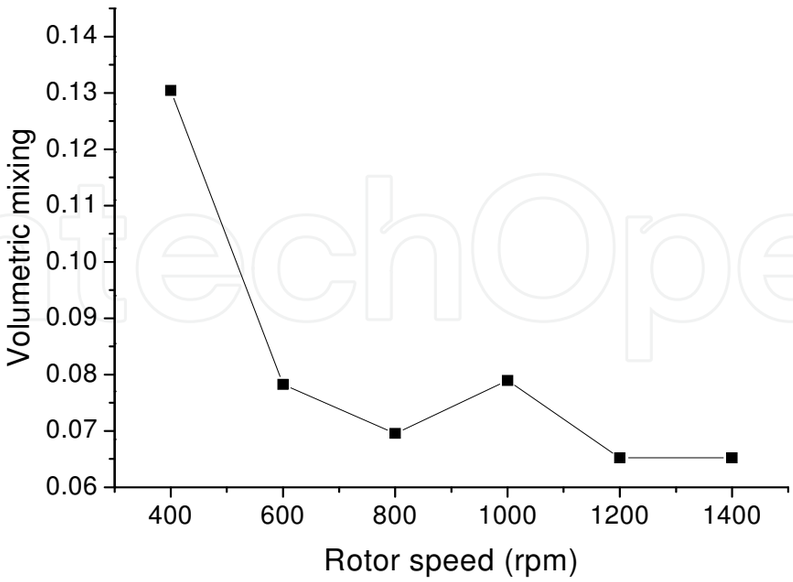

Fig. 7. Relationship between rotor speed and mixing rate

3. Face seal of RPE

Fig.8 shows the seal structure of assembled RPE which is composed of rotor, end covers and sleeve. A set of rings made of 316L is used to adjust clearance in experiment. The center shaft is used to assembly the above components and it will not affect the face clearance because there is no radial contact between center shaft and seal components. The materials of rotor and end covers are cemented carbide and the planarity and parallelism are ensured through precious surface finishing. The clearance can be adjusted by changing different rings from 0.02mm to 0.13mm.

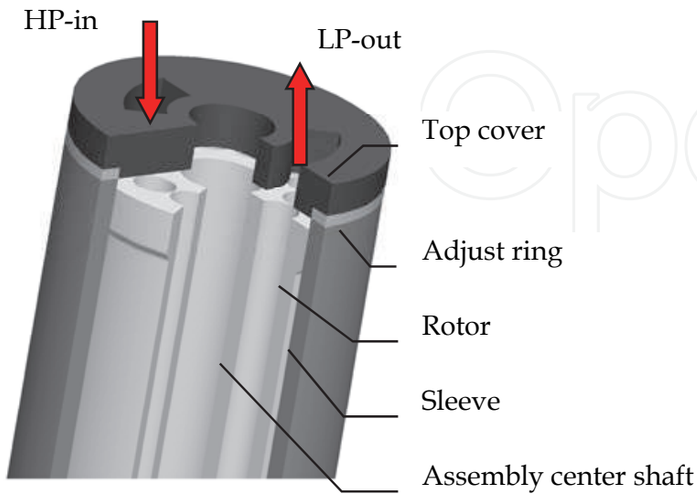

Fig. 8. Face seal structure of RPE

Fig.8 is the front view of axial RPE. The fluid distributors on the end-covers are designed to release the flow shock caused by the suddenly contact between high pressure fluid and low pressure ones. The fluid enters the clearance through seal surface, which is the most significant difference from typical mechanical seal.

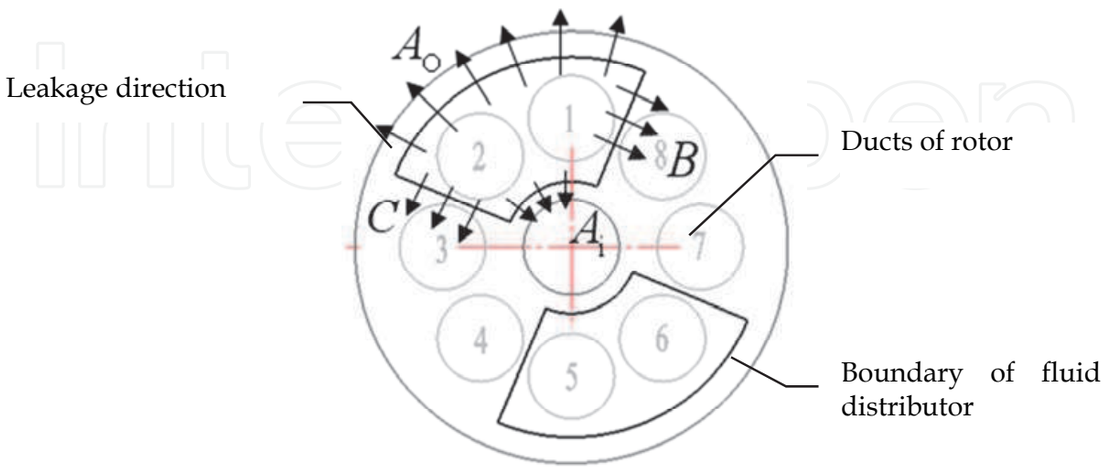

Fig. 9. Flow direction in clearance

Fig. 9. is the top view of RPE and shows the boundary of fluid distributor. Number1~8 are the ducts of rotor when rotating. The arrows illustrate the leakage after fluid entering the clearance whose direction is normal to the boundary

Generally speaking, the face seal structure of RPE has its own special characteristics:

1. There is constant flow crossing seal surface into the seal clearance.
2. There are leakages both at radial and at tangential direction from high pressure side to low pressure side.
3. The shear flow caused by relative rotating could be parallel or perpendicular to pressure-driven flow caused by pressure gradient. Moreover, when these two kinds of flows are parallel they could be at same direction or at opposite direction.

Therefore, face seal of RPE is much more complicated than traditional mechanical seal technology. However, the study on it in this paper could be done from both theoretical analysis and experiments ways.

3.1 Numerical simulation on face seal of RPE

3.1.1 Hypothesis

There are several hypotheses for the face seal numerical simulation.

1. The velocity at the thickness direction $\upsilon_Z = 0$
2. The high pressure fluid entering the clearance will flow at the direction normal to the boundary of fluid distributor to low pressure side.
3. There is no thermal effect during face sealing.

3.1.2 Geometry model and boundary conditions

Fig.10 is the geometry model of clearance between rotor and end cover with arrows illustrate the flow direction in hypothesis. Fig.11 is the grid display.

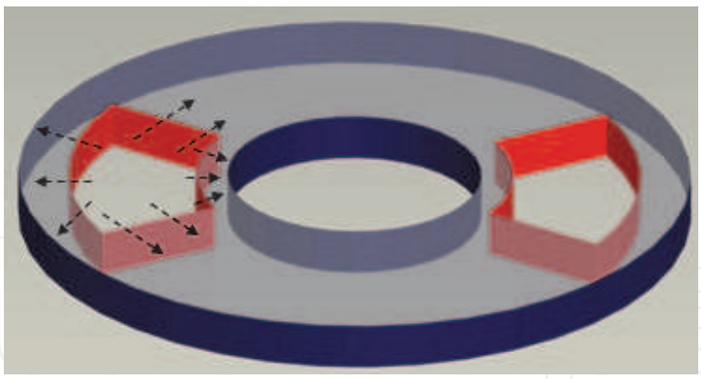

Fig. 10. Geometry model of clearance (not to scale)

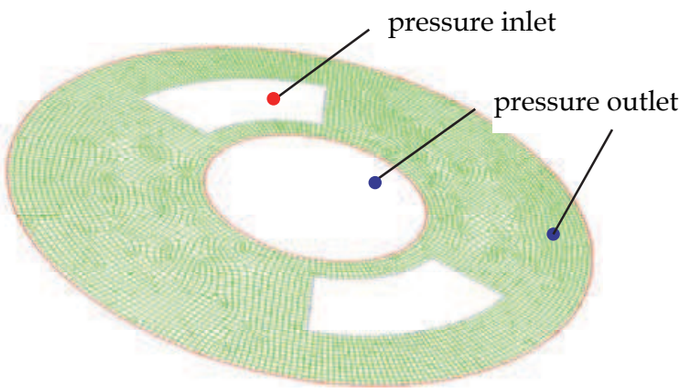

Fig. 11. Gridded geometry model

The red surfaces in Fig.10 are defined as pressure-inlet and $p = 6.0\text{MPa}$. The blue surfaces are defined as pressure-outlet and $p = 0.2\text{MPa}$.

3.1.3 Governing equations

The numerical simulation is carried out under cylindrical coordination. And the governing equations are[4,5],

$$\text{Continuity Equation} \qquad \frac{1}{r}\frac{\partial(r\upsilon_r)}{\partial r}+\frac{1}{r}\frac{\partial(\upsilon_\theta)}{\partial\theta}=0 \tag{10}$$

Momentum Equation
Radial direction:

$$\rho\left(\frac{\partial\upsilon_r}{\partial t}+\upsilon_r\frac{\partial\upsilon_r}{\partial r}+\frac{\upsilon_\theta}{r}\frac{\partial\upsilon_r}{\partial\theta}-\frac{\upsilon_\theta^2}{r}\right)=\rho f_r-\frac{\partial p}{\partial r}+\mu\left[\frac{\partial}{\partial r}\left(\frac{1}{r}\frac{\partial}{\partial r}(r\upsilon_r)\right)+\frac{1}{r^2}\frac{\partial^2\upsilon_r}{\partial\theta^2}-\frac{2}{r^2}\frac{\partial\upsilon_\theta}{\partial\theta}\right] \tag{11}$$

Tangential direction:

$$\rho\left(\frac{\partial\upsilon_\theta}{\partial t}+\upsilon_r\frac{\partial\upsilon_\theta}{\partial r}+\frac{\upsilon_\theta}{r}\frac{\partial\upsilon_\theta}{\partial\theta}+\frac{\upsilon_\theta\upsilon_r}{r}\right)=\rho f_\theta-\frac{1}{r}\frac{\partial p}{\partial\theta}+\mu\left[\frac{\partial}{\partial r}\left(\frac{1}{r}\frac{\partial}{\partial r}(r\upsilon_\theta)\right)+\frac{1}{r^2}\frac{\partial^2\upsilon_\theta}{\partial\theta^2}-\frac{2}{r^2}\frac{\partial\upsilon_r}{\partial\theta}\right] \tag{12}$$

The energy equation is not necessary because of hypothesis (3).

3.2 Simulation results and discussion

3.2.1 Verification of model validity

Firstly, the validity of simulation model was verified through comparison with experimental results. Fig.12 is the comparison between simulation results and experimental ones.

The maximum difference between simulation results and experimental ones is 0.02m^3/h and the minimum one is 0.004m^3/h, which ensured the model valid to guide the experiments and engineering design.

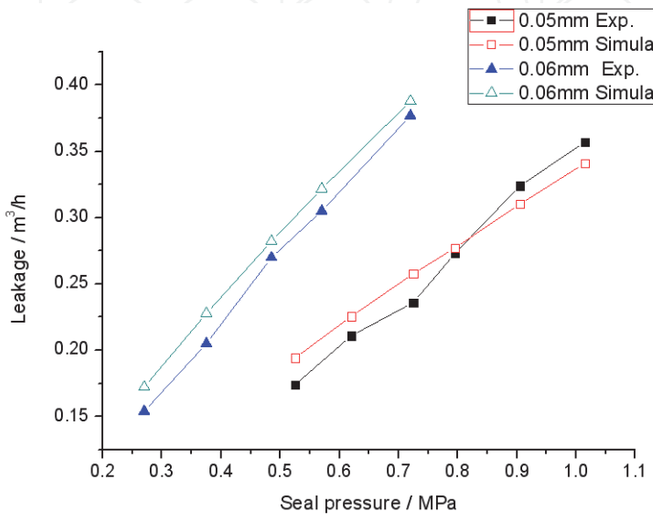

Fig. 12. Comparison between simulation results and experimental ones

3.2.2 pressure distribution in clearance

Fig.13 shows the liquid film pressure distribution in clearance.

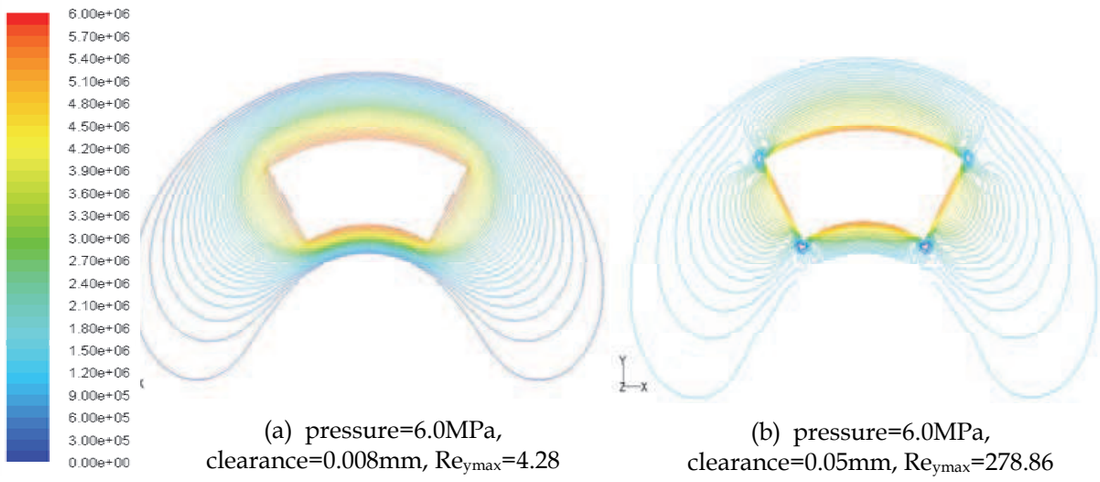

(a) pressure=6.0MPa, clearance=0.008mm, Re_{ymax}=4.28

(b) pressure=6.0MPa, clearance=0.05mm, Re_{ymax}=278.86

Fig. 13. Pressure distribution in clearance

Fig.13 illustrates the totally different form of face seal at different clearance. It could be seen that pressure is well sealed when laminar flow in the clearance shown in (a). However, the

Reynolds number increased with the increasing of clearance and the turbulence occurred at the boundary which makes the seal pressure decreased dramatically shown in (b) and means the seal has been destroyed.

3.2.3 Effects of rotor speed on leakage

Fig.14 shows the variation of leakage with rotor speed at 0.02mm and seal pressure is 6.0MPa. It could be seen that the leakage has little changed with the rotor speed increasing from 600rpm to 1600rpm, which means the rotor has no effects on leakage. The results were accordance with the theoretical computations and could be explained that the rotor speed has no effects on flux crossing boundary A and its effects on boundary B and C cancelled each other. Therefore the rotor speed has no effects on total leakage.

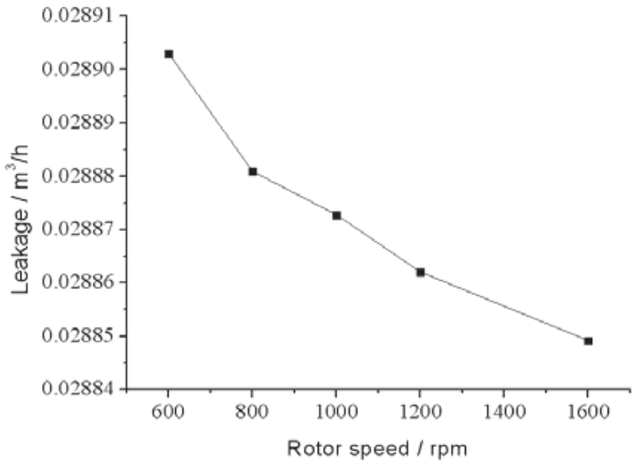

Fig. 14. Relationship between leakage and rotor speed

3.2.4 Effects of clearance on seal pressure and pressure

Fig.15 shows the relationship between clearance and seal pressure at different flux.

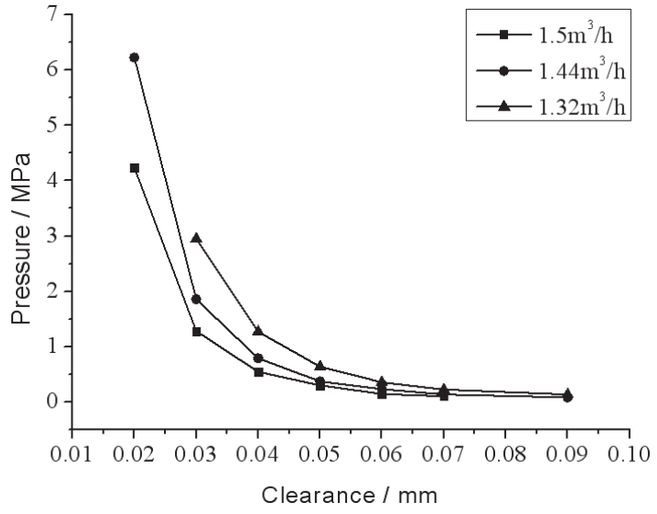

Fig. 15. Relationship between clearance and pressure

It could be seen from Fig.15 that the seal pressure decreased dramatically with the increasing of clearance especially when the clearance is less than 0.03mm. Under different flux when the clearance is larger than 0.04mm the seal pressure will be less than 1MPa which can not meet the requirements of SWRO operation. Therefore, the clearance should be controlled to as minimum as possible while keeping rotor rotating, otherwise the more flux is needed to makeup leakage loss.
Fig.16 shows the relationship between clearance and leakage at different seal pressure.

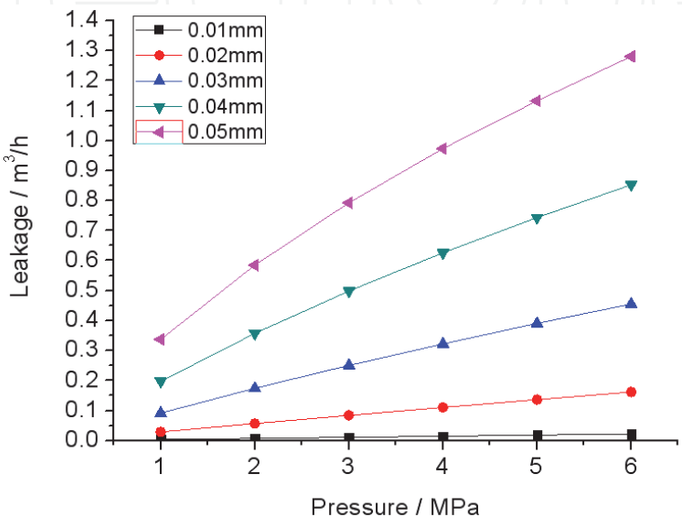

Fig. 16. Relationship between clearance, pressure and leakage

It could be seen that the leakage increases more rapidly at larger clearance than that does at smaller one. If the clearance of RPE could not be controlled under 0.01mm the pressure requirements for SWRO operation have to be met at the cost of increasing flux, which consequently leads to the flow unbalance into and out of RPE.

4. Energy recovery experiment with RPE

4.1 Design of noncontact face seal structure

The face seal structure of RPE in the experimental RPE is shown in Fig.17. The face seal structure is composed of rotor, end covers and sleeve. A set of rings with different thickness is used to adjust clearance between rotor and end covers in RPE.
In Fig.17, h_1 and h_2 are the height of rotor and sleeve respectively. h_3 is the thickness of adjust ring. h_4 and h_5 are the assembly height of top and bottom end cover respectively.
The clearance is controlled in the order of 10^{-2} mm and to 0.02mm as its minimum through adjustable ring with different thickness during energy recovery experiments. When the clearance is less than 0.02mm the rotor of RPE will not start driven by jet flow under experimental conditions. During SWRO energy recovery experiments, the clearance is adjusted to minimum at first step as long as the rotor could start. And then mixing rate, face leakage and energy recovery efficiency are evaluated through salinity, pressure and flux data.

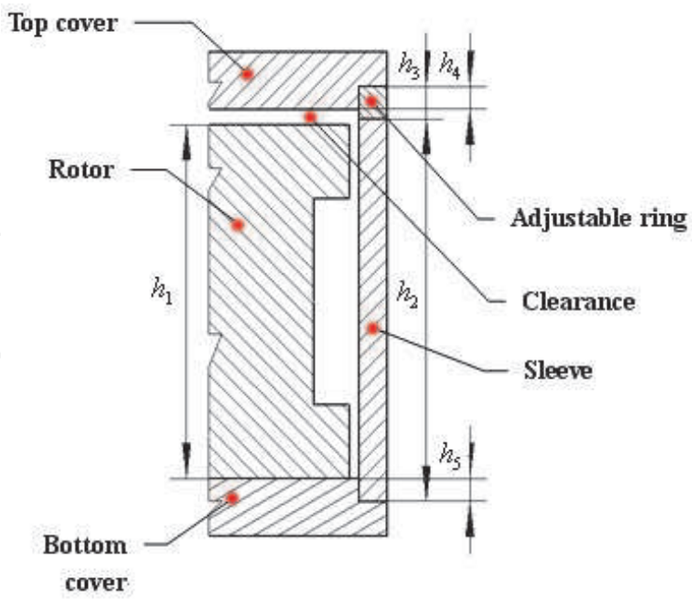

Fig. 17. Noncontact seal structure of RPE unit

4.2 RPE unit

Fig.18 is the RPE unit in the experimental study. The materials of rotor, end covers and sleeve are carefully chosen to counteract corrosion of NaCl solution. The face materials of rotor and end covers are cemented carbide and the planarity and parallelism are ensured through precious surface finishing.

The rotor is driven by external jet flow to start up. The rotor speed could be adjusted through changing the orifice diameter of jet.

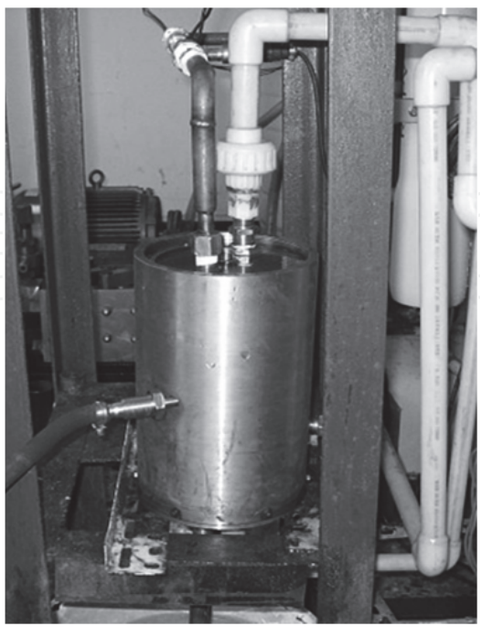

Fig. 18. RPE unit driven by fluid

4.3 Design of SWRO experimental system

Fig.19 is the scheme of RPE energy recovery experiment system with seawater reverse osmosis (SWRO). The capacity of SWRO is 1.2m^3/h and the salt rejection is over 99% and recovery rate is 40%. The purity of production water is monitored by conductivity. The pressure in front of the reverse osmosis is adjusted by throttle valve (V5) and monitored by pressure gauge (P5).

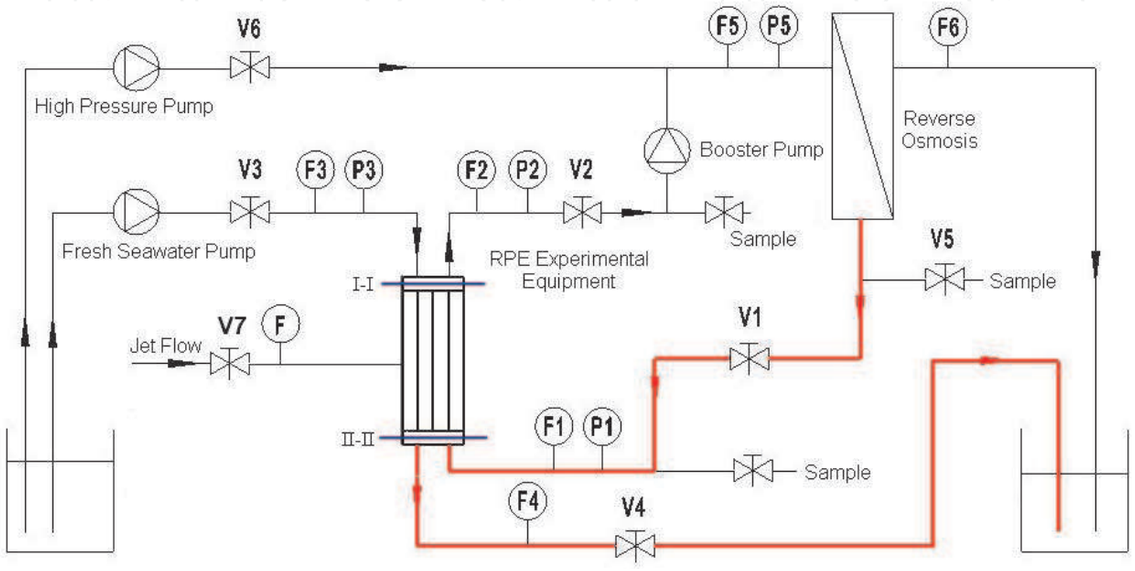

P— pressure gauges or sensors F— flux meters or sensors V—Valve

Fig. 19. SWRO experimental system scheme

The pressure and flow rate are measured and recorded through pressure sensors and flow meters at the pipes from and to the RPE experimental unit. Moreover, there are three sampling points which are used to salinity measurement during experiments. The rotor speed is adjusted through orifice diameter. The configuration of valves is designed to make face seal performance, mixing rate, energy recovery and their relationship being studied.

4.4 Experimental procedure

According to Fig.19 the V1~V4 are initially closed. Firstly the SWRO system starts and operation pressure can be adjusted through V7. Secondly, rotor of RPE driven by jet flow starts and then the booster pump and V1~V4 open to assemble the RPE into the SWRO system.

4.5 Experimental results and discussion

4.5.1 Face seal performance

In this experiment, tap water is used as experimental fluids. Fig.20 shows the characteristics of face seal at different clearance in experiments. It could be seen that the face seal has better performance at smaller clearance than larger one.

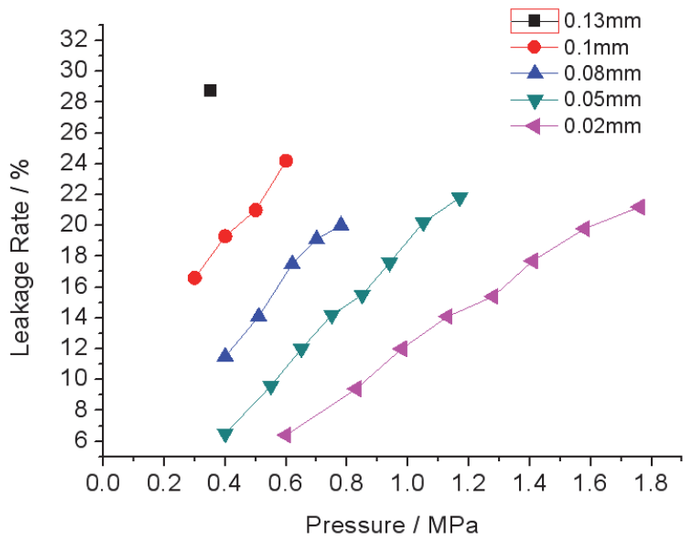

Fig. 20. Relationship between system pressure and leakage rate at different clearances

Fig.21 shows the relationship between pressure and clearance. It is clear that with the increasing of clearance the system pressure deceases and leakage increases dramatically. And when the clearance is larger than 0.1mm the leakage will so unbearable that the SWRO system has lost operation.

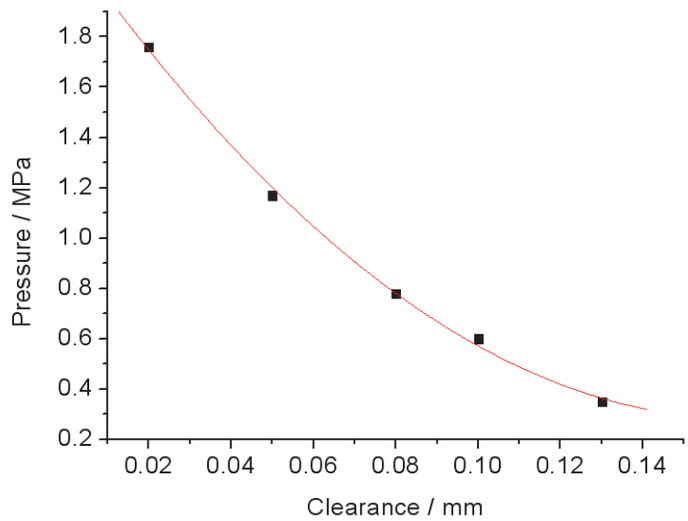

Fig. 21. Relationship of system pressure and clearance

Fig.22 shows the relationship between energy recovery efficiency and clearance. It could be seen that the energy recovery efficiency decreases with the increasing of clearance.
The face seal experiments demonstrate that its performance plays a very important role in the operation of RPE. The larger clearance makes the leakage increase and the SWRO lost normal operation point.

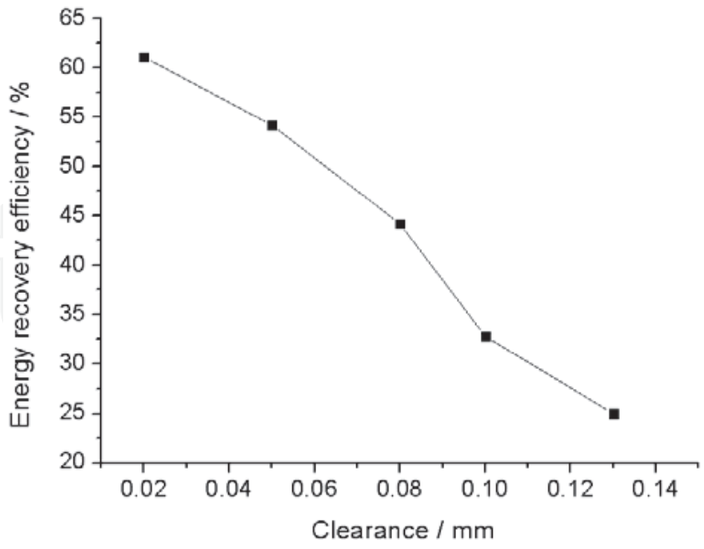

Fig. 22. Relationship of clearance and energy recovery efficiency

4.5.2 Mixing rate and energy recovery experiments

In this experiment, the NaCl solution is used to replace real seawater as experimental fluid. The main purpose of this part is to study characteristics of mixing during energy recovery process.

The experimental results are listed in Tab.1.

Experiments	Item	Low pressure inlet	High pressure outlet	High pressure inlet	Low pressure outlet	Mixing Rate	Energy recovery efficiency
1	Pressure (MPa)	0.1	0.53	0.83	0		
	Flow Rate (L/min)	20.5	20	21.4	22		
	Electric Conductivity (mS/cm)	47.3	42.1	25.9	26.3		
	Salinity (%)	4.79	4.71	2.21	2.26	3.16%	53.5%
2	Pressure (MPa)	0.1	0.87	1.15	0		
	Flow Rate (L/min)	22.5	20	21.4	24.1		
	Electric Conductivity (mS/cm)	47.3	42.1	25.9	26.3		
	Salinity (%)	4.79	4.71	2.21	2.26	3.16%	64.8%
3	Pressure (MPa)	0.1	1.07	1.41	0		
	Flow Rate (L/min)	24.5	20.4	22	26.3		
	Electric Conductivity (mS/cm)	46.9	42.2	26.1	26.4		
	Salinity (%)	4.76	4.71	2.21	2.26	2%	65.3%
4	Pressure (MPa)	0.1	1.42	1.76	0		
	Flow Rate (L/min)	25.5	20.6	23.5	27.4		
	Electric Conductivity (mS/cm)	47.2	42.2	23.4	26.4		
	Salinity (%)	4.79	4.71	2.24	2.24	3.14%	66.7%

Table 1. Experiments of energy recovery with different fluid

It could be seen from the Tab.1 that the mixing rate is well controlled less than 3.5%. However, because the clearance is only 0.02mm the serious leakage deteriorates the face seal performance. The seal pressure decreased dramatically and the energy recovery efficiency was not satisfactory.

5. Conclusion

The effective control of mixing rate in the ducts of rotor is very important to the stable operation of SWRO. The 3D mixing model is setup in the paper and the conclusions are as following:

1. The liquid piston is formed and moves reciprocally in the ducts. And the fresh seawater is separated by the liquid piston to be prevented from over-mixing with brine.
2. The flow-in velocity and rotor speed are the most important parameters affecting mixing rate. The mixing rate will increase with increasing of flow-in velocity.
3. The mixing rate will almost keep stable even the rotor speed increases once the rotor speed is more than 800rpm.

At the same time, excellent face seal plays very important role in separating the high pressure system from low pressure of RPE in order to ensure the normal operation of SWRO. The characteristics of face seal and relationship between clearance, pressure and leakage are studied through theoretical analysis, numerical simulation and experimentally studied in the paper. The conclusions are as following:

1. Laminar flow in clearance makes the face seal reliable. When the turbulent flow occurs the pressure gradient and face seal are destroyed.
2. Rotor speed has no obvious effects on the leakage in face seal process.
3. The seal pressure decreases and leakage increases dramatically with the increasing of clearance. The clearance should be controlled less than 0.01mm for the SWRO operation.
4. The pressure decreases and leakage increases dramatically with the increasing of clearance. The clearance in RPE is controlled to 0.02mm as minimum. Under such clearance the mixing rate of different concentration NaCl solutions is less than 3.5%. However the larger clearance leads to deterioration of face seal, building up pressure and energy recovery efficiency. Although the highest energy recovery efficiency is just 66.7% the experimental study clearly illustrates the face seal between rotor and end cover is the MOST important factor in RPE energy transfer process.

6. References

[1] Zhou Yihui etc. Numerical simulation on dynamic mixing process in duct of RPE, Desalination and Water Treatment,2009.1
[2] Zhou Yihui. Theoretical and experimental study on energy recovery process of RPE in SWRO(D),Dalian University of Technology,2010
[3] User Manual PX45s, Energy Recovery Inc. USA 2006
[4] ANSYS FLUENT 12.0 user's guide FLUENT Inc., 2006
[5] G. K. Batchelor. An Introduction to Fluid Dynamics. Cambridge Univ. Press, Cambridge, England, 1967
[6] ANSYS FLUENT 12.0 user's guide(section 12.4.2, section 7.5, section7.10, section 7.13.1). FLUENT Inc., 2006,

[7] B. E. Launder and D. B. Spalding. Lectures in Mathematical Models of Turbulence. Academic Press, London, England, 1972.
[8] R.L. Stover, Development of a fourth generation energy recovery device. Desalination, 165 (2004) 313–321
[9] Victor L. Streeter, E. Benjamin Wylie, Keith W. Bedford. Fluid Mechanics (9th edition) [M].McGraw Hill Publish
[10] John D. Anderson, Jr. Computational Fluid Mechanics-The Basics with Applications [M].McGraw Hill PublishC. Fritzmann, J. Löwenberg, T. Wintgens, T. Melin. State-of-the-art of reverse osmosis desalination. Desalination 216 (2007) 1–76

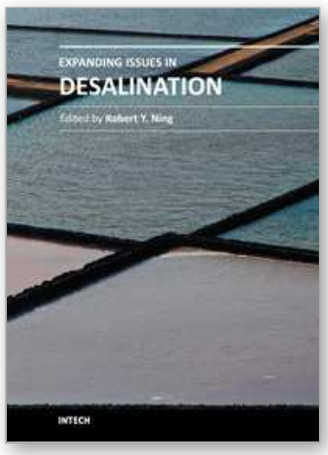

Expanding Issues in Desalination

Edited by Prof. Robert Y. Ning

ISBN 978-953-307-624-9
Hard cover, 412 pages
Publisher InTech
Published online 22, September, 2011
Published in print edition September, 2011

For this book, the term â€œdesalinationâ€ is used in the broadest sense of the removal of dissolved, suspended, visible and invisible impurities in seawater, brackish water and wastewater, to make them drinkable, or pure enough for industrial applications like in the processes for the production of steam, power, pharmaceuticals and microelectronics, or simply for discharge back into the environment. This book is a companion volume to â€œDesalination, Trends and Technologiesâ€, INTECH, 2011, expanding on the extension of seawater desalination to brackish and wastewater desalination applications, and associated technical issues. For students and workers in the field of desalination, this book provides a summary of key concepts and keywords with which detailed information may be gathered through internet search engines. Papers and reviews collected in this volume covers the spectrum of topics on the desalination of water, too broad to delve into in depth. The literature citations in these papers serve to fill in gaps in the coverage of this book. Contributions to the knowledge-base of desalination is expected to continue to grow exponentially in the coming years.

How to reference

In order to correctly reference this scholarly work, feel free to copy and paste the following:

Zhou Yihui, Bi Mingshu and Liu Yu (2011). Rotary Pressure Exchanger for SWRO, Expanding Issues in Desalination, Prof. Robert Y. Ning (Ed.), ISBN: 978-953-307-624-9, InTech, Available from: http://www.intechopen.com/books/expanding-issues-in-desalination/rotary-pressure-exchanger-for-swro

INTECH
open science | open minds

InTech Europe
University Campus STeP Ri
Slavka Krautzeka 83/A
51000 Rijeka, Croatia
Phone: +385 (51) 770 447
Fax: +385 (51) 686 166
www.intechopen.com

InTech China
Unit 405, Office Block, Hotel Equatorial Shanghai
No.65, Yan An Road (West), Shanghai, 200040, China
中国上海市延安西路65号上海国际贵都大饭店办公楼405单元
Phone: +86-21-62489820
Fax: +86-21-62489821

IntechOpen